Acta Crystallographica Section D
Biological Crystallography
ISSN 0907-4449

Structure of a thermophilic cyanobacterial b_6f-type Rieske protein

Sebastian Veit,[a] Kazuki Takeda,[b] Yuichi Tsunoyama,[c] Dorothea Rexroth,[a] Matthias Rögner[a]* and Kunio Miki[b]*

[a]Plant Biochemistry, Ruhr University Bochum, 44780 Bochum, Germany, [b]Department of Chemistry, Graduate School of Science, Kyoto University, Sakyo-ku, Kyoto 606-8502, Japan, and [c]Division of Biology, Radioisotope Research Center, Kyoto University, Sakyo-ku, Kyoto 606-8502, Japan

Correspondence e-mail: matthias.roegner@rub.de, miki@kuchem.kyoto-u.ac.jp

Received 10 May 2012
Accepted 31 July 2012

PDB Reference: TePetC, 3azc

The 'Rieske protein' PetC is one of the key subunits of the cytochrome b_6f complex. Its Rieske-type [2Fe–2S] cluster participates in the photosynthetic electron-transport chain. Overexpression and careful structure analysis at 2.0 Å resolution of the extrinsic soluble domain of PetC from the thermophilic cyanobacterium *Thermosynechococcus elongatus* BP-1 enabled in-depth spectroscopic and structural characterization and suggested novel structural features. In particular, both the protein structure and the positions of the internal water molecules unexpectedly showed a higher similarity to eukaryotic PetCs than to other prokaryotic PetCs. The structure also revealed a deep pocket on the PetC surface which is oriented towards the membrane surface in the whole complex. Its surface properties suggest a binding site for a hydrophobic compound and the complete conservation of the pocket-forming residues in all known PetC sequences indicates the functional importance of this pocket in the cytochrome b_6f complex.

1. Introduction

Rieske proteins are essential subunits of all classes of cytochrome *bc*-type complexes and play a key role in photosynthetic and respiratory electron-transport processes (see, for example, Link, 2001). The Rieske protein PetC is a subunit of the cytochrome b_6f complex and contains a 2Fe–2S cluster with a midpoint redox potential of about +300 mV (see, for example, Bernát & Rögner, 2011; Baniulis *et al.*, 2008; Kallas, 2011; Crofts *et al.*, 2000). PetC transfers one electron from plastoquinol to the cytochrome *f* subunit of the complex. Participation of the Rieske 2Fe–2S cluster in the accompanying proton transfer has also been suggested (Crofts *et al.*, 2000).

As in other cyanobacteria, the cytochrome b_6f complex in *Thermosynechococcus elongatus* BP-1 (*T. elongatus*) participates in both respiratory and photosynthetic electron transport as the central intersection point between the two processes. Its significance for regulation is also indicated by the fact that multiple *petC* genes have been reported for several cyanobacterial strains (Schneider *et al.*, 2002, 2004; Yan & Cramer, 2003; for a review, see Schneider & Schmidt, 2005). This multiplicity (up to four *petC* genes) enables adaptation to stress conditions such as high light (Tsunoyama *et al.*, 2009), low oxygen (Summerfield *et al.*, 2008) or the high demand for reduction equivalents during nitrogen assimilation (Schneider & Schmidt, 2005; Arnold, 2001). In contrast, *T. elongatus* contains only a single *petC* gene coding for PetC1, in analogy to all photosynthetic eukaryotes (Schneider *et al.*, 2004). Structurally, all PetC proteins consist of an extrinsic soluble domain which is connected to an N-terminal

transmembrane helix by a flexible hinge. Although crystal structures of both prokaryotic and eukaryotic cytochrome b_6f complexes have been analyzed up to about 3 Å resolution (Baniulis *et al.*, 2009; Yamashita *et al.*, 2007; Kurisu *et al.*, 2003; Stroebel *et al.*, 2003), this resolution is not sufficient to visualize details such as the positions of water molecules, which may be important for modelling functional mechanisms on a molecular level. In contrast, high-resolution structures (1.9 Å) are available for the soluble domain of cytochrome *f* from both prokaryotic and eukaryotic sources (Carrell *et al.*, 1999; Chi *et al.*, 2000; Martinez *et al.*, 1996). This high resolution revealed a buried chain of five water molecules with possible relevance for proton translocation. In the case of PetC, a 1.83 Å resolution structure is available of the extrinsic C-terminal domain of spinach Rieske protein (Carrell *et al.*, 1997). However, a high-resolution structure of cyanobacterial PetC is still lacking.

Here, we report detailed spectroscopic and crystallographic analyses of the soluble domain of PetC from the thermophilic cyanobacterium *T. elongatus* (Nakamura *et al.*, 2002; Yamaoka *et al.*, 1978) which has been heterologously expressed. The high resolution of these crystallographic data revealed the positions of structurally important internal water molecules and enabled their comparison with the corresponding water molecules in the eukaryotic structure from spinach. We also present for the first time a putative ligand-binding pocket on the surface of PetC from *T. elongatus*. Conservation of this pocket in all other available PetC structures suggests a new regulatory mechanism for the cytochrome b_6f complex.

2. Materials and methods

2.1. Cloning, expression and purification of recombinant TePetC

The gene fragment encoding the soluble domain (residues 54–180) of the Rieske protein of *T. elongatus* (TePetC) was amplified from *T. elongatus* genomic DNA by PCR using the primers ATCTGTGGTCTCTGCGCGCGGTTGCCAAGGATGCTTT and ATCGCCGGTCTCTTATCATTACGTCCACCAAGGTTCTTTG to generate *Bsa*I sites at the 5′- and 3′-termini. Using these *Bsa*I restriction sites, the PCR fragment was inserted into pASK-IBA37plus (IBA GmbH) to generate the respective expression plasmid. The recombinant protein was designed to have 16 additional residues (MASRGSHHHHHHIEGR) at the N-terminus with a His_6 tag and a factor Xa restriction site. Transformed *Escherichia coli* cells (Rosetta, Novagen) were grown at 310 K in LB medium containing 100 µg ml^{-1} ampicillin to an optical density (OD_{600}) of 0.6. Overexpression was then induced by 200 µg l^{-1} anhydrotetracycline and after 4–5 h cultivation cells were harvested by centrifugation (4000*g* for 30 min and 277 K). All further steps were performed at 277 K. Cell pellets were suspended in buffer *A* (50 m*M* Tris–HCl pH 8.0, 0.5 m*M* EDTA, 100 m*M* NaCl), pelleted by centrifugation (see above) and suspended in buffer *B* (50 m*M* NaH_2PO_4 pH 8.0, 300 m*M* NaCl, 10 m*M* imidazole) supplemented with protease inhibitors [1:100; protease-inhibitor cocktail (EDTA-free), Nacalai Tesque] and lysozyme (1 mg ml^{-1}). After incubation for 30 min on ice, the cells were lysed by sonication. The cell lysate was centrifuged (14 000*g* for 30 min at 277 K) and the filtered supernatant was loaded onto an Ni–NTA column (Qiagen; 2.5 ml Ni–NTA resin per litre of culture) equilibrated with buffer *B*. A dark brown colour of the column indicated binding of recombinant Rieske protein to the Ni–NTA resin. After washing with 25 ml buffer *C* (50 m*M* NaH_2PO_4 pH 8.0, 300 m*M* NaCl, 20 m*M* imidazole) per litre of resin, bound protein was eluted with buffer *D* (50 m*M* NaH_2PO_4 pH 8.0, 300 m*M* NaCl, 250 m*M* imidazole), which was immediately replaced by buffer *F* (10 m*M* Tris–HCl pH 7.3) *via* ultrafiltration (Amicon Ultra 10K). As several trials failed to remove the His_6 tag by digestion with factor Xa protease, His-tagged protein variants were used for all experiments.

Recombinant TePetC was further purified by gel-filtration chromatography using a Superdex 75 column (GE Healthcare) equilibrated with buffer *E* (10 m*M* Tris–HCl pH 7.3, 150 m*M* NaCl). The main peak fractions containing monomeric TePetC were collected and the buffer was replaced by buffer *F* (see above). The concentrated protein solution (54 mg ml^{-1} protein concentration) was frozen in liquid nitrogen and stored at 193 K.

2.2. Spectroscopic measurements

The absorption spectra of oxidized [by addition of 5 m*M* $K_2Fe(CN)_6$] or reduced (by addition of 5 m*M* DTT) TePetC (0.7 mg ml^{-1}) in buffer *F* were recorded at room temperature (298 K) in a V-630 spectrometer (Jasco).

Circular-dichroism (CD) spectra were recorded in a quartz cuvette with 1.0 mm path length at 293–373 K between 190 and 250 nm in 1 nm increments (bandwidth of 2 nm) using a J-715 CD spectropolarimeter (Jasco). The spectra represent averages of three scans using TePetC (∼0.24 mg ml^{-1}) in 5 m*M* potassium phosphate buffer pH 7.5. The thermal melting point (T_m) of the protein was estimated by plotting the CD data at 222 nm against temperature followed by fitting to a Boltzmann sigmoidal curve between 348 and 367 K.

2.3. Crystallization and structure determination

The sitting-drop vapour-diffusion method was used with 54 mg ml^{-1} TePetC in buffer *F* and reservoir solution consisting of 18%(*w*/*v*) PEG 3000, 9%(*v*/*v*) 2-propanol, 18.5%(*v*/*v*) glycerol and 90 m*M* Na HEPES pH 8.0 in a 2:1 ratio. Crystallization drops were equilibrated against 500 µl reservoir solution at 293 K, yielding hexagonal crystals (maximal dimensions 0.5 × 0.5 × 0.3 mm) within one week. All diffraction experiments were performed on BL41XU at SPring-8 (Harima, Japan) using an MX225HE detector (Rayonix) , a beam size of 50 × 50 µm and an original photon flux of 4 × 10^{11} photons s^{-1} at the sample position. Data collection was performed using 0.65 Å X-rays with reduction of the initial flux density to 1/25 by an aluminium attenuator of 3.0 mm thickness using helium gas at 40 K for cooling. 180 frames of diffraction images were collected with an oscillation

Table 1
Crystallographic and refinement statistics.

Values in parentheses are for the highest resolution shell.

Crystal data	
Space group	$P6_5$
Unit-cell parameters (Å)	a = 91.3, c = 43.3
Resolution range (Å)	25–2.0 (2.13–2.00)
Reflections (total/unique)	98082/12341
Multiplicity	7.9 (5.6)
Completeness (%)	87.4 (57.1)
$\langle I/\sigma(I)\rangle$	32.2 (2.1)
$R_{\rm merge}$† (%)	7.6 (47.1)
Refinement	
Residues in asymmetric unit	133
Heterogeneous molecules	1 × 2Fe–2S, 98 × H_2O
Total atoms	1134
$R_{\rm work}$‡/$R_{\rm free}$§ (%)	19.7/23.6
R.m.s.d. bonds (Å)/angles (°)	0.009/1.5
Average B factor (Å^2)	
Protein	57.3
Ligands [2Fe–2S]	48.4
Water/Wat202	66.6/40.6
Ramachandran statistics of φ/ψ angles	
Residues in favoured regions	126 [96.2%]
Residues in allowed regions	4 [3.1%]
Outliers	1 [0.8%]
PDB code	3azc

† $R_{\rm merge} = \sum_{hkl}\sum_i |I_i(hkl) - \langle I(hkl)\rangle|/\sum_{hkl}\sum_i I_i(hkl)$. ‡ $R_{\rm work} = \sum_{hkl} ||F_{\rm obs}| - |F_{\rm calc}||/\sum_{hkl}|F_{\rm obs}|$. § $R_{\rm free}$ was calculated using 5% of the reflections that were not included in the refinement as a test set.

Table 2
Crystallographic statistics of data sets collected at two different wavelengths near the iron K absorption edge.

Values in parentheses are for the highest resolution shell.

	High energy	Low energy
Data collection		
Wavelength (Å)	1.730	1.750
X-ray energy (eV)	7166	7085
f'' (e$^-$) (S/K/Ca/Fe)	0.7/1.3/1.6/4.0	0.7/1.3/1.6/0.5
Crystal data		
Space group	$P6_5$	$P6_5$
Unit-cell parameters (Å)	a = 91.5, c = 43.0	a = 91.5, c = 43.1
Resolution range (Å)	30–2.5 (2.59–2.50)	30–2.5 (2.59–2.50)
Reflections (total/unique)	66060/6965	67058/7086
Multiplicity	9.5 (9.6)	9.5 (9.5)
Completeness (%)	95.8 (76.7)	97.4 (83.0)
$\langle I/\sigma(I)\rangle$	54.9 (13.1)	57.5 (14.2)
$R_{\rm merge}$† (%)	10.8 (24.0)	10.2 (22.3)

† $R_{\rm merge} = \sum_{hkl}\sum_i |I_i(hkl) - \langle I(hkl)\rangle|/\sum_{hkl}\sum_i I_i(hkl)$.

angle of 1.0° and an exposure time of 0.5 s per frame. The absorption dose was estimated with *RADDOSE* (Murray *et al.*, 2004) and additional data sets for the detection of anomalous signal were collected at wavelengths of 1.73 and 1.75 Å. Processing and scaling of the diffraction data sets was performed using the *HKL*-2000 software package (Otwinowski & Minor, 1997). The crystals belonged to space group $P6_5$, with unit-cell parameters $a = b = 91.3$, $c = 43.3$ Å. The crystal structure was solved by molecular replacement using *MOLREP* (Vagin & Teplyakov, 2010) in the *CCP*4 suite (Winn *et al.*, 2011) using the coordinates of the Rieske domain of the b_6f complex from *Mastigocladus laminosus* (PDB entry 2e74; Yamashita *et al.*, 2007) as the search model. Starting from an initial model autotraced using the *ARP/wARP* program (Perrakis *et al.*, 1999), the output structure was manually improved and refined using *XtalView* and *CNS* (McRee, 1999; Brünger *et al.*, 1998). The final structure was validated with *RAMPAGE* (Lovell *et al.*, 2003). Data-collection and refinement statistics are shown in Tables 1 and 2. Isoelectric points

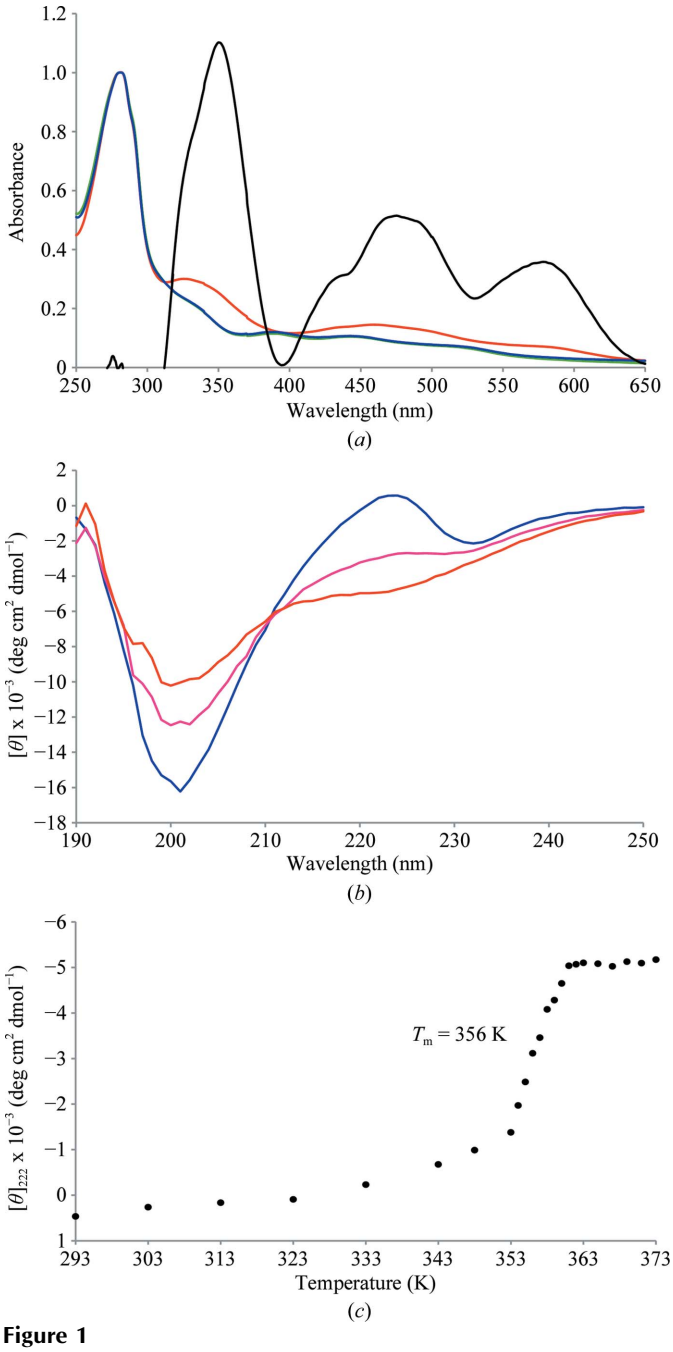

Figure 1
Spectroscopic analyses of TePetC. (*a*) UV–Vis spectra for nontreated (0.7 mg ml^{-1}; green line), artificially reduced (blue line) and oxidized samples (red line); scaling is according to the 280 nm absorbance of the nontreated sample, with the difference spectra ($A_{\rm ox} - A_{\rm red}$) shown as black lines (with a tenfold magnification). (*b*) UV (190–250 nm) region of the CD spectra at 293 K (blue), 356 K (pink) and 373 K (red). (*c*) Temperature-dependent unfolding of TePetC according to CD at 222 nm. The thermal melting point, T_m, was determined by a Boltzmann sigmoidal curve fitted to data between 348 and 367 K.

(pI) were calculated using the *Compute pI/Mw* tool of the ExPASy server (Gasteiger *et al.*, 2005). Figures of molecular models were prepared using the *PyMOL* program (DeLano, 2002). Coordinates and structure factors for TePetC have been deposited in the Protein Data Bank (PDB entry 3azc).

3. Results and discussion

3.1. Purification and spectroscopic characterization of TePetC

Heterologous overexpression of the soluble part of PetC from *T. elongatus* (TePetC) in *E. coli* and subsequent purification by affinity and size-exclusion chromatography yielded about 50 mg per litre of *E. coli* culture. The concentrated protein solution was deep red-brown, which is typical for iron–sulfur proteins. Redox changes were accompanied by characteristic changes in the absorption spectrum, with maxima at 351, 475 and 579 nm in the oxidized minus reduced difference spectrum (Fig. 1*a*; Link, 2001). The fact that the spectrum of the nontreated sample was almost identical to the spectrum of the artificially reduced sample indicates that the purified Rieske proteins were mainly in the reduced state. From CD spectra (Fig. 1*b*) recorded at different temperatures a T_m of 356 K was calculated (Fig. 1*c*), indicating the remarkable stability of the protein structure. The UV CD spectrum of TePetC, with a maximum at 224 nm and two minima at 200 and 232 nm (Fig. 1*b*), is atypical of proteins which consist predominantly of β-sheets. However, similar CD spectra have been reported for other small β-sheet-dominated proteins (see, for example, Knapp *et al.*, 1998). These features may be caused by aromatic side chains, which have been shown to strongly affect UV CD spectra (Freskgård *et al.*, 1994).

The construction of a truncated TePetC variant without the transmembrane domain and hinge region but with a His tag fused to the amino-terminus enabled large-scale heterologous overexpression of this redox-active protein. In contrast to previous reports (Holton *et al.*, 1996; Schneider *et al.*, 2000; Gubernator *et al.*, 2003), our system does not require an additional refolding process or reconstruction of the iron–sulfur cluster; this reduces the likelihood of artifacts in protein folding considerably.

3.2. Crystal structure

Data collection was performed under a low X-ray dose with cryocooling at 40 K to avoid X-ray-radiation-induced bias (see, for example, Yano *et al.*, 2005; De la Mora *et al.*, 2012) in the TePetC structure. The dose per frame and the total dose were estimated to be 5.5×10^2 and 1.0×10^5 Gy, respectively, with the latter being smaller than the Henderson limit (Henderson, 1990) by more than two orders of magnitude. Diffraction spots could be observed to 1.9 Å resolution along the a^* and b^* axes, but only to 2.3 Å resolution along the c^* axis. The resolution of the data set was determined to be 2.0 Å, while the highest resolution shell had a relatively low completeness owing to the anisotropic diffraction. However, the electron density was improved upon the inclusion of diffraction data from the highest resolution shell. Finally, the R_{work} and R_{free} factors converged to 19.7% and 23.6%,

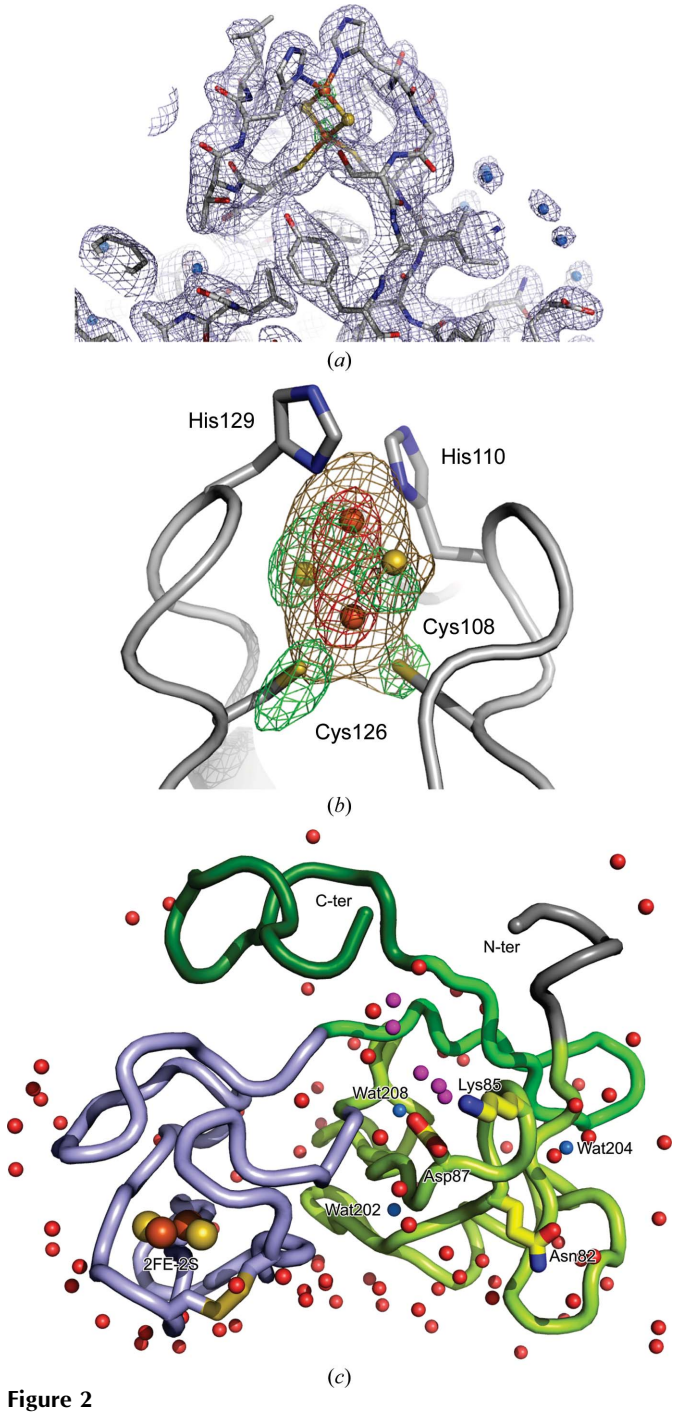

Figure 2
Structure of TePetC. (*a*) σ_A-Weighted $2F_o - F_c$ map contoured at the 1.0σ and 10σ levels as a grey and a green mesh, respectively. (*b*) Anomalous difference Fourier map (λ = 1.73 Å) at the 3.0σ level (beige mesh) and the 10σ level (red mesh); an additional map (λ = 1.75 Å) is shown at the 3.0σ level (green mesh). (*c*) Overall structure and subdomain architecture of TePetC: iron-binding subdomain (residues 105–149, light blue) and large subdomain (residues 54–104, light green; residues 150–165, green; residues 166–180, deep green), with additional residues at the N-terminus (grey). Water molecules are shown on the protein surface (red spheres), as internal molecules (blue) and as a buried water cluster in the putative ligand-binding pocket (pink; see §3.5). The side chains of Asn82, Lys85 and Asp87 in the protruding loop are shown as stick models.

respectively (Table 1). The high-resolution electron-density map allowed the determination of exact conformations of the side chains and of the positions of water molecules (Fig. 2*a*).

The existence, positions and identities of heavy atoms was examined by anomalous difference Fourier maps which were calculated from data sets collected using X-rays of 1.73 and 1.75 Å wavelength, respectively (Table 2). These wavelengths correspond to high- and low-energy remotes of the *K* absorption edge of iron at 1.7433 Å. Strong densities were observed in the anomalous difference Fourier map at 1.73 Å in the vicinity of Cys108, His110, Cys126 and His129, while the corresponding map at 1.75 Å showed no strong density at these positions (Fig. 2*b*). However, weaker densities for S atoms could be observed in both data sets. These results indicate that the two heavy atoms which were coordinated by these residues and by two additional S atoms were unambiguously iron. We therefore conclude that the Rieske-type 2Fe–2S cluster is properly integrated into the protein from the *E. coli* cells without any additional treatment.

The soluble part of TePetC consists of an Fe–S cluster-binding subdomain and a large subdomain with three clusters of residues: amino acids 54–104, 150–165 and 166–180 (Fig. 2*c*). Among them, the C-terminal residues (166–180) are highly conserved in all b_6f-type Rieske homologues, while they are completely absent in other types of Rieske proteins. The secondary structure of TePetC is dominated by β-sheets, similar to other PetC1 proteins. However, the structures of the cyanobacterial and eukaryotic PetCs differ in detail, which may lead to functional and/or regulatory differences.

3.3. Structural comparison of TePetC with other PetCs

Structural superposition of TePetC and other PetCs leads to root-mean-square deviation (r.m.s.d.) values of 0.7–1.4 Å for corresponding C^{α} atoms (Fig. 3*a*). Unexpectedly, superpositions with SoPetC from *Spinacia oleracea* (spinach; PDB entry 1rfs; Carrell *et al.*, 1997) and CrPetC from the green alga *Chlamydomonas reinhardtii* (PDB entry 1q90; Stroebel *et al.*, 2003) revealed smaller r.m.s.d. values than those with other cyanobacterial PetCs, including MlPetC from the thermophilic cyanobacterium *Mastigocladus laminosus* (PDB entry 2e74;

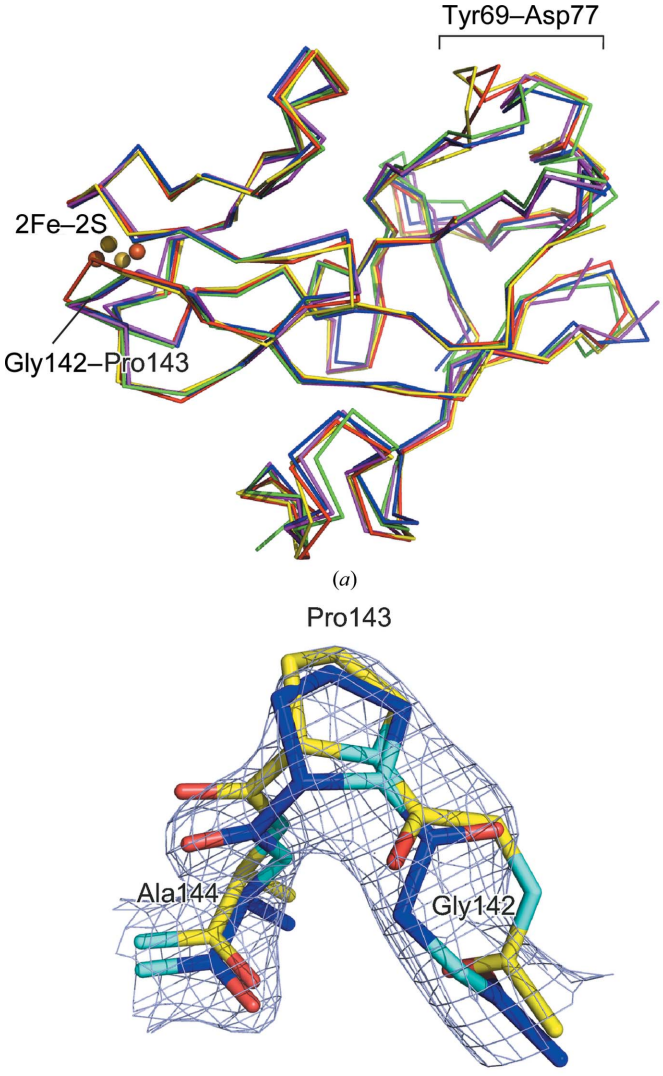

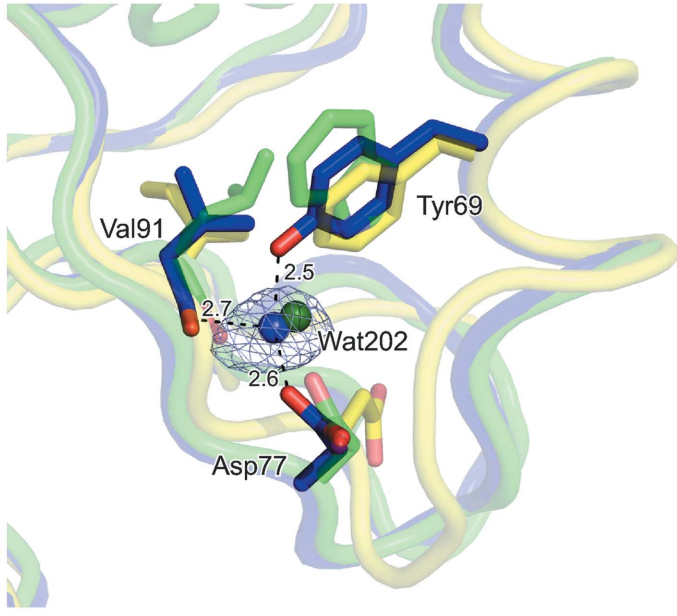

Figure 3
Structural comparison with other PetC proteins. (*a*) Structures of PetC from *T. elongatus* (blue; this work), *S. oleracea* (green; PDB entry 1rfs; r.m.s.d. 0.7 Å; 65.6% residue identity), *C. reinhardtii* (magenta; PDB entry 1q90; r.m.s.d. 0.8 Å; 70.1% residue identity), *M. laminosus* (yellow; PDB entry 2e74; r.m.s.d. 1.2 Å; 68.5% residue identity) and *Nostoc* sp. PCC 7120 (red; PDB entry 2zt9; r.m.s.d. 1.1 Å; 68.5% residue identity) shown as C^{α} models. Residue numbering is according to TePetC. (*b*) *Cis*-peptide bond between Gly142 and Pro143 of the TePetC structure (blue) superimposed with the corresponding *trans*-peptide bond of PetC from *M. laminosus* (yellow) as stick models. A σ_A-weighted $2F_o - F_c$ map for the TePetC structure contoured at 2.0σ is shown as a grey mesh. (*c*) Internal water molecule (Wat202) coordinated by the side chains of Tyr69 (distance 2.5 Å) and Asp77 (2.6 Å) and the main-chain carbonyl of Val91 (2.7 Å). For comparison, PetC structures from a higher plant (*S. oleracea*; green) and from another cyanobacterium (*M. laminosus*; yellow) are shown. The OMIT map of Wat202 is contoured at 3.0σ as a grey mesh. Anomalous difference Fourier maps at long wavelengths (λ = 1.73 and 1.75 Å) showed no electron-density peaks (4σ levels) at the position of Wat202.

Yamashita *et al.*, 2007). These differences in the r.m.s.d. values mainly arise from residues Tyr69–Asp77 and the fact that a *cis*-peptide bond occurs at Gly142-Pro143 exclusively in eukaryotic PetCs and TePetC (Fig. 3*b*).

Thermophilic and mesophilic PetC proteins show no apparent differences in the numbers of hydrogen bonds, hydrophobic interactions or disulfide bridges. However, the thermophilic PetCs from *T. elongatus* and *M. laminosus* have a more neutral pI than most PetCs from mesophilic cyanobacteria, indicating differences in the protein surface charge. It has been shown in previous studies that the exchange of only a few surface-exposed residues can result in considerably increased thermostability of a protein owing to electrostatic stabilization (Pace, 2000; Perl *et al.*, 2000). Additional salt bridges (Kumar *et al.*, 2000; Taylor & Vaisman, 2010), long-range coulombic interactions (Grimsley *et al.*, 1999; Perl *et al.*, 2000) and the elimination of unfavourable electrostatic repulsion (Perl *et al.*, 2000) can contribute to such stabilization. As the crystal structures of the thermophilic TePetC and the mesophilic SoPetC show the same number of salt bridges, the latter two may contribute to the increased thermal stability of TePetC. We also identified additional internal water molecules in the TePetC structure (Wat202, Wat204 and Wat208) which are partly absent in the corresponding mesophilic proteins. In summary, both the presence of internal water molecules and the charge-altering mutation of specific surface-exposed residues could considerably increase the T_m of thermophilic PetC variants.

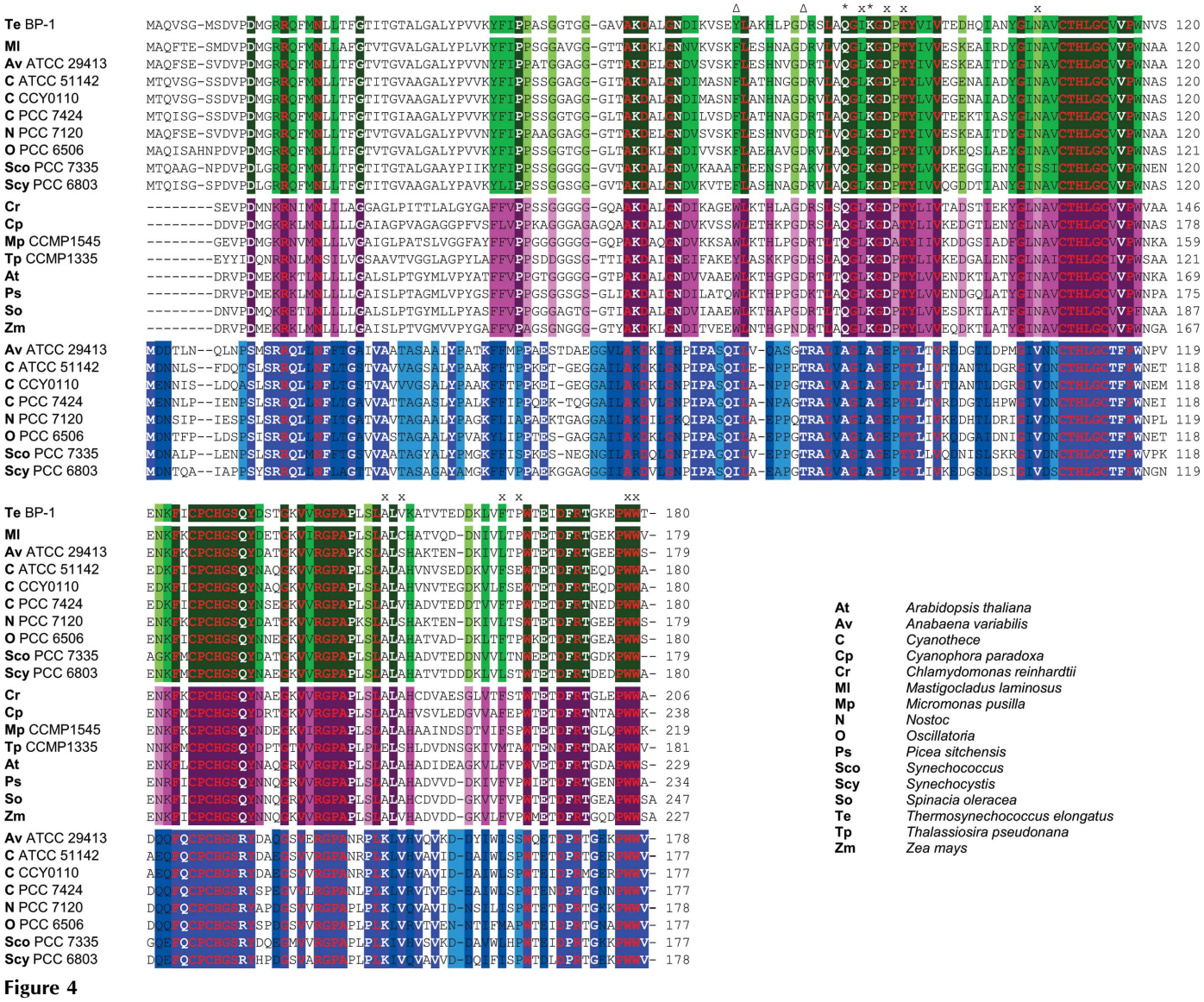

Figure 4
Sequence alignment of PetCs from various species. Apart from the two thermophilic cyanobacteria *T. elongatus* BP-1 and *M. laminosus*, all species are mesophilic. Fully, highly and relatively conserved residues among the cyanobacterial species are shaded dark green, green and light green, respectively. Alignments of PetC from eukaryotes (shaded pink) and PetC2 from cyanobacteria (shaded blue) are also shown for comparison [the alternative Rieske protein of *Anabaena variabilis* ATCC 29413 is part of the PetC4 group (Schneider & Schmidt, 2005; Arnold, 2001), which shows a high sequence similarity to the PetC2 group]. The following symbols are used in the alignments: X for residues of the pocket wall, an asterisk for residues in the protruding loop next to the pocket and Δ for residues involved in binding of Wat202. Sequence alignment was performed using *ClustalW*2 (Larkin *et al.*, 2007).

3.4. Structurally important water molecules

The crystal structure of TePetC contained 85 water molecules (Fig. 2*c*), of which three have been assigned as internal water molecules (Wat202, Wat204 and Wat208). These water molecules are completely surrounded by the protein matrix and might be important for both protein structure and function. Notably, the $F_o - F_c$ map revealed an unusual strong electron-density peak at the position corresponding to Wat202, which could indicate the presence of a metal ion at this site (Fig. 3*c*). Calcium and potassium could be excluded by anomalous difference Fourier maps at long wavelengths (λ = 1.73 and 1.75 Å) and atomic emission spectroscopy of the purified protein (data not shown). Also, owing to the coordination geometry of Wat202 (Harding, 2002, 2006), a sodium ion is very unlikely at this position. In order to find differences in the internal water molecules in structures from higher plants and prokaryotes, our high-resolution prokaryotic structure was compared with the corresponding eukaryotic structure from spinach (PDB entry 1rfs; Carrell *et al.*, 1997). Owing to their low resolution, water molecules could not be resolved in other PetC crystal structures (Baniulis *et al.*, 2009; Yamashita *et al.*, 2007; Stroebel *et al.*, 2003) and hence they did not help in this comparison. Our analysis showed that Wat204 and Wat208 are (with small deviations) coordinated by main-chain atoms. Wat204 (for simplicity, TePetC numbering is used) does not exist in the SoPetC crystal structure. In the TePetC structure Wat204 is coordinated by the backbone carbonyl O atom of Ile64 and the amine group of Leu161, whereas the corresponding atoms in the SoPetC structure are directly connected by a hydrogen bond. Although the presence or absence of this internal water molecule is not correlated with strong structural changes, it may have an impact on protein stability, as has been shown for many other proteins (see, for example, Luntz *et al.*, 1989; Helms, 2007; Takano *et al.*, 1997). The third internal water molecule in the TePetC structure, Wat202, is coordinated by the side chains of Tyr69 and Asp77 and the main-chain carbonyl of Val91. Surprisingly, in other cyanobacterial PetC1s Tyr69 is usually replaced by Phe (Fig. 4), which is unable to form a hydrogen bond to the water molecule (Fig. 3*c*). Assuming that at least three hydrogen bonds are necessary to bury a water molecule

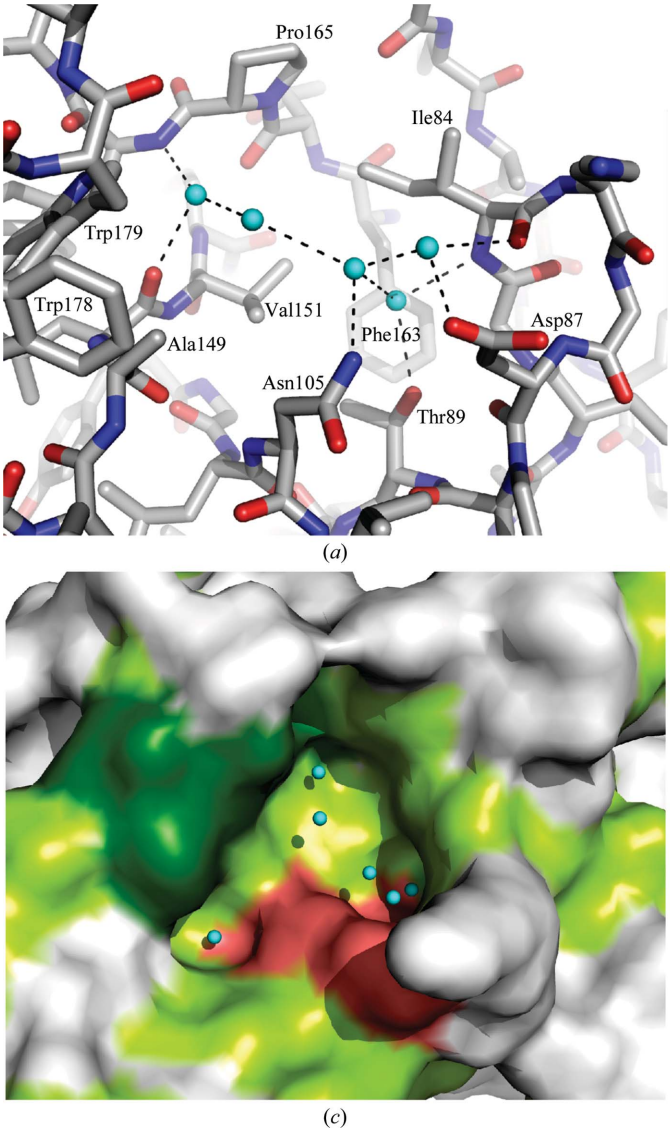

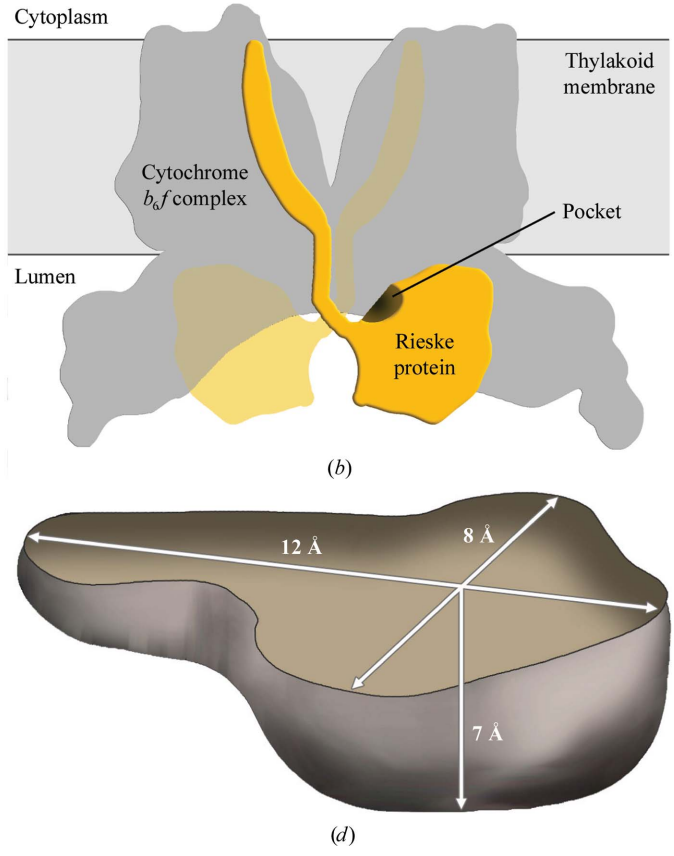

Figure 5
View of the putative ligand-binding site. (*a*) Hydrogen-bonding network of the water cluster filling the pocket. (*b*) Model of the dimeric cytochrome b_6f complex in the thylakoid membrane with the Rieske protein (yellow) and its pocket (highlighted as a dark spot). (*c*) Surface representation of the pocket, with aromatic (Phe, Trp and Tyr; green), hydrophobic (Ala, Cys, Ile, Leu, Pro and Val; light green) and hydrophilic residues (at the edge, *i.e.* Asp87, Thr89 and Asn105; pale red) indicated. (*d*) Schematic model with the approximate dimensions of the pocket.

(Rashin *et al.*, 1986), this replacement will result in the loss of this internal water molecule. In contrast, in SoPetC Tyr69 is replaced by Trp, which also enables the binding of a water molecule (Fig. 3*c*). Since eukaryotic PetCs generally contain Trp69 or Tyr69 and Asp77 (Fig. 4), the internal water molecule Wat202 should be fully conserved in eukaryotes. The superposition of prokaryotic and eukaryotic PetCs (Fig. 3*a*) indicates a significant role of Wat202 in the conformation of residues Tyr69–Asp77. Also, the complete conservation of Wat202 in eukaryotes suggests a function of this internal water molecule within the eukaryotic cytochrome b_6f complex.

3.5. The surface pocket as a putative ligand-binding site

The protein surface of TePetC revealed a deep pocket which is located at the junction of the cluster-binding subdomain and the large subdomain, and is filled by a cluster of water molecules (Fig. 5*a*). This pocket was also detected by the *metaPocket* software for the identification of ligand-binding sites (Huang, 2009). In the structure of the whole cytochrome b_6f complex the pocket is oriented towards the membrane surface on the lumen side (Fig. 5*b*). It most probably forms a ligand-binding site which is highly hydrophobic inside (owing to residues Ile84, Ala149, Val151, Phe163, Pro165, Trp178 and Trp179) and hydrophilic at the edge (owing to residues Asp87, Thr89 and Asn105) (Figs. 5*a*, 5*c* and 5*d*). These residues are completely or highly conserved in PetC1 (Fig. 4). A buried cluster of water molecules as seen in Fig. 5(*a*) may be fixed by the hydrophilic interior of this pocket. It is possible that this water easily dissociates upon complex formation with a ligand. The fact that mainly C-terminal residues (Trp166–Thr180) contribute to the formation of this pocket may account for its absence and presence in respiratory-type (Iwata *et al.*, 1996; Hunsicker-Wang *et al.*, 2003) and b_6f-type Rieske proteins, respectively (Baniulis *et al.*, 2009; Yamashita *et al.*, 2007; Stroebel *et al.*, 2003; Carrell *et al.*, 1997). Also, the presence of an empty pocket in all available crystal structures of cytochrome b_6f complexes indicates a transient and/or weak interaction with the potential binding partner. The discovery of a membrane-facing hydrophobic pocket suggests the binding of a lipophilic ligand, which may be a plastoquinone, chlorophyll or carotenoid.

Asp87 (Fig. 5*a*), which is located at the edge of the pocket as part of a protruding loop (Fig. 2*c*), is also a putative interaction site with the hinge region or another transmembrane element of the cytochrome b_6f complex. Interestingly, this residue and two other well conserved residues of this loop, Asn82 and Lys85 (Fig. 2*c*), are replaced in PetC2 and PetC4 (Fig. 4). This may have a serious impact on the ligand-binding properties of the pocket.

4. Conclusions

The Rieske protein TePetC is a key subunit of the cytochrome b_6f complex from the thermophilic cyanobacterium *T. elongatus*. In this study, we overexpressed the soluble domain of TePetC in its redox-active holo form followed by detailed spectroscopic and crystallographic characterizations. Owing to the high-resolution (2.0 Å) crystal structure, three internal water molecules with potential impact on the stability and function of the protein could be resolved for the first time for cyanobacterial PetC. While one of them is completely conserved in all known eukaryotic PetCs, it is missing in all other known cyanobacterial PetCs. Also, the conformation of loop Tyr69–Asp77 and the presence of a *cis*-peptide bond at Gly142-Pro143 confirm the similarities between TePetC and eukaryotic PetCs. The fact that protein structures are usually more conserved than amino-acid sequences (Holm & Sander, 1996) indicates that higher plant chloroplasts may originate from a cyanobacterium closely related to *T. elongatus*.

We also discovered a putative hydrophobic ligand-binding pocket on the TePetC protein surface which may regulate electron transport from plastoquinone to cytochrome *f*. While previous studies have indicated the importance of conformational changes ('tethered diffusion') in this step (Yan & Cramer, 2003; Yu *et al.*, 2008), it is still unclear how this sensing mechanism could be triggered.

In conclusion, the well resolved structure of the thermophilic cyanobacterial Rieske protein reported in this study may stimulate new structure-based approaches to clarify both the evolution and the regulation of electron-transport processes within the cytochrome b_6f complex.

We gratefully acknowledge the critical input of and careful reading of the manuscript by Dr Gabor Bernat and Dr Sascha Rexroth (RUB). We also greatly appreciate the help of the beamline staff at SPring-8 and the financial support of the Industrialized Countries Instrument Education Cooperation Programme (ICI-ECP), which enabled a stay of SV at Kyoto University. This work was also supported by Grants in Aid for Scientific Research from MEXT of Japan (to KT and KM).

References

Arnold, M. (2001). Doctoral dissertation. University of Regensburg, Germany.

Baniulis, D., Yamashita, E., Whitelegge, J. P., Zatsman, A. I., Hendrich, M. P., Hasan, S. S., Ryan, C. M. & Cramer, W. A. (2009). *J. Biol. Chem.* **284**, 9861–9869.

Baniulis, D., Yamashita, E., Zhang, H., Hasan, S. S. & Cramer, W. A. (2008). *Photochem. Photobiol.* **84**, 1349–1358.

Bernát, G. & Rögner, M. (2011). *Bioenergetic Processes of Cyanobacteria*, edited by G. A. Peschek, C. Obinger & G. Renger, pp. 573–606. Dordrecht: Springer.

Brünger, A. T., Adams, P. D., Clore, G. M., DeLano, W. L., Gros, P., Grosse-Kunstleve, R. W., Jiang, J.-S., Kuszewski, J., Nilges, M., Pannu, N. S., Read, R. J., Rice, L. M., Simonson, T. & Warren, G. L. (1998). *Acta Cryst.* D**54**, 905–921.

Carrell, C. J., Schlarb, B. G., Bendall, D. S., Howe, C. J., Cramer, W. A. & Smith, J. L. (1999). *Biochemistry*, **38**, 9590–9599.

Carrell, C. J., Zhang, H., Cramer, W. A. & Smith, J. L. (1997). *Structure*, **5**, 1613–1625.

Chi, Y.-I., Huang, L.-S., Zhang, Z., Fernández-Velasco, J. G. & Berry, E. A. (2000). *Biochemistry*, **39**, 7689–7701.

Crofts, A. R., Guergova-Kuras, M., Kuras, R., Ugulava, N., Li, J. & Hong, S. (2000). *Biochim. Biophys. Acta*, **1459**, 456–466.

De la Mora, E., Lovett, J. E., Blanford, C. F., Garman, E. F., Valderrama, B. & Rudino-Pinera, E. (2012). *Acta Cryst.* D**68**, 564–577.
DeLano, W. L. (2002). *PyMOL*. http://www.pymol.org.
Freskgård, P. O., Mårtensson, L. G., Jonasson, P., Jonsson, B. H. & Carlsson, U. (1994). *Biochemistry*, **33**, 14281–14288.
Gasteiger, E., Hoogland, C., Gattiker, A., Duvaud, S., Wilkins, M. R., Appel, R. D. & Bairoch, A. (2005). *The Proteomics Protocols Handbook*, edited by J. M. Walker, pp. 571–607. Totowa: Humana Press.
Grimsley, G. R., Shaw, K. L., Fee, L. R., Alston, R. W., Huyghues-Despointes, B. M., Thurlkill, R. L., Scholtz, J. M. & Pace, C. N. (1999). *Protein Sci.* **8**, 1843–1849.
Gubernator, B., Seidler, A., Rögner, M. & Szczepaniak, A. (2003). *Protein Expr. Purif.* **29**, 8–14.
Harding, M. M. (2002). *Acta Cryst.* D**58**, 872–874.
Harding, M. M. (2006). *Acta Cryst.* D**62**, 678–682.
Helms, V. (2007). *ChemPhysChem*, **8**, 23–33.
Henderson, R. (1990). *Proc. R. Soc. London Ser. B*, **241**, 6–8.
Holm, L. & Sander, C. (1996). *Science*, **273**, 595–603.
Holton, B., Wu, X., Tsapin, A. I., Kramer, D. M., Malkin, R. & Kallas, T. (1996). *Biochemistry*, **35**, 15485–15493.
Huang, B. (2009). *OMICS*, **13**, 325–330.
Hunsicker-Wang, L. M., Heine, A., Chen, Y., Luna, E. P., Todaro, T., Zhang, Y. M., Williams, P. A., McRee, D. E., Hirst, J., Stout, C. D. & Fee, J. A. (2003). *Biochemistry*, **42**, 7303–7317.
Iwata, S., Saynovits, M., Link, T. A. & Michel, H. (1996). *Structure*, **4**, 567–579.
Kallas, T. (2011). *Photosynthesis: Plastid Biology, Energy Conversion and Carbon Assimilation*, edited by J. J. Eaton-Rye, B. C. Tripathy & T. D. Sharkey, pp. 501–560. Dordrecht: Springer.
Knapp, S., Mattson, P. T., Christova, P., Berndt, K. D., Karshikoff, A., Vihinen, M., Smith, C. I. & Ladenstein, R. (1998). *Proteins*, **31**, 309–319.
Kumar, S., Tsai, C.-J., Ma, B. & Nussinov, R. (2000). *J. Biomol. Struct. Dyn.* **17**, 79–85.
Kurisu, G., Zhang, H., Smith, J. L. & Cramer, W. A. (2003). *Science*, **302**, 1009–1014.
Larkin, M. A., Blackshields, G., Brown, N. P., Chenna, R., McGettigan, P. A., McWilliam, H., Valentin, F., Wallace, I. M., Wilm, A., Lopez, R., Thompson, J. D., Gibson, T. J. & Higgins, D. G. (2007). *Bioinformatics*, **23**, 2947–2948.
Link, T. A. (2001). *Handbook of Metalloproteins*, edited by A. Messerschmidt, R. Huber, T. L. Poulos & K. Weighardt, pp. 518–531. New York: Wiley.
Lovell, S. C., Davis, I. W., Arendall, W. B. III, de Bakker, P. I., Word, J. M., Prisant, M. G., Richardson, J. S. & Richardson, D. C. (2003). *Proteins*, **50**, 437–450.
Luntz, T. L., Schejter, A., Garber, E. A. & Margoliash, E. (1989). *Proc. Natl Acad. Sci. USA*, **86**, 3524–3528.
Martinez, S. E., Huang, D., Ponomarev, M., Cramer, W. A. & Smith, J. L. (1996). *Protein Sci.* **5**, 1081–1092.
McRee, D. E. (1999). *J. Struct. Biol.* **125**, 156–165.
Murray, J. W., Garman, E. F. & Ravelli, R. B. G. (2004). *J. Appl. Cryst.* **37**, 513–522.
Nakamura, Y. *et al.* (2002). *DNA Res.* **9**, 123–130.
Otwinowski, Z. & Minor, W. (1997). *Methods Enzymol.* **276**, 307–326.
Pace, C. N. (2000). *Nature Struct. Biol.* **7**, 345–346.
Perl, D., Mueller, U., Heinemann, U. & Schmid, F. X. (2000). *Nature Struct. Biol.* **7**, 380–383.
Perrakis, A., Morris, R. & Lamzin, V. S. (1999). *Nature Struct. Biol.* **6**, 458–463.
Rashin, A. A., Iofin, M. & Honig, B. (1986). *Biochemistry*, **25**, 3619–3625.
Schneider, D., Berry, S., Volkmer, T., Seidler, A. & Rögner, M. (2004). *J. Biol. Chem.* **279**, 39383–39388.
Schneider, D., Jaschkowitz, K., Seidler, A. & Rögner, M. (2000). *Indian J. Biochem. Biophys.* **37**, 441–446.
Schneider, D. & Schmidt, C. L. (2005). *Biochim. Biophys. Acta*, **1710**, 1–12.
Schneider, D., Skrzypczak, S., Anemüller, S., Schmidt, C. L., Seidler, A. & Rögner, M. (2002). *J. Biol. Chem.* **277**, 10949–10954.
Stroebel, D., Choquet, Y., Popot, J. L. & Picot, D. (2003). *Nature (London)*, **426**, 413–418.
Summerfield, T. C., Toepel, J. & Sherman, L. A. (2008). *Biochemistry*, **47**, 12939–12941.
Takano, K., Funahashi, J., Yamagata, Y., Fujii, S. & Yutani, K. (1997). *J. Mol. Biol.* **274**, 132–142.
Taylor, T. J. & Vaisman, I. I. (2010). *BMC Struct. Biol.* **10**, S5.
Tsunoyama, Y., Bernát, G., Dyczmons, N. G., Schneider, D. & Rögner, M. (2009). *J. Biol. Chem.* **284**, 27875–27883.
Vagin, A. & Teplyakov, A. (2010). *Acta Cryst.* D**66**, 22–25.
Winn, M. D. *et al.* (2011). *Acta Cryst.* D**67**, 235–242.
Yamaoka, T., Satoh, K. & Katoh, S. (1978). *Plant Cell Physiol.* **19**, 943–954.
Yamashita, E., Zhang, H. & Cramer, W. A. (2007). *J. Mol. Biol.* **370**, 39–52.
Yan, J. & Cramer, W. A. (2003). *J. Biol. Chem.* **278**, 20925–20933.
Yano, J., Kern, J., Irrgang, K. D., Latimer, M. J., Bergmann, U., Glatzel, P., Pushkar, Y., Biesiadka, J., Loll, B., Sauer, K., Messinger, J., Zouni, A. & Yachandra, V. K. (2005). *Proc. Natl Acad. Sci. USA*, **102**, 12047–12052.
Yu, C.-A., Cen, X., Ma, H.-W., Yin, Y., Yu, L., Esser, L. & Xia, D. (2008). *Biochim. Biophys. Acta*, **1777**, 1038–1043.